

1-Sulfonyl-4-acylpiperazines as Selective Cannabinoid-1 Receptor (CB1R) Inverse Agonists for the Treatment of Obesity

Petr Vachal,^{*,†} Joan M. Fletcher,[†] Tung M. Fong,[‡] Cathy C. R.-R. Huang,[‡] Julie Lao,[‡] Jing C. Xiao,[‡] Chun-Pyn Shen,[‡] Alison M. Strack,[§] Lauren Shearman,[§] Sloan Stribling,[§] Richard Z. Chen,[‡] Andrea Frassetto,[‡] Xinchun Tong,^{||} Junying Wang,^{||} Richard G. Ball,[⊥] Nancy N. Tsou,[⊥] Gerard J. Hickey,[§] Donald F. Thompson,[§] Terry D. Faidley,[§] Susan Nicolich,[§] Joana Achanfuo-Yeboah,[§] Donald F. Hora,[§] Jeffrey J. Hale,[†] and William K. Hagmann[†]

Departments of Medicinal Chemistry, Metabolic Diseases, Pharmacology, Drug Metabolism/Pharmacokinetics, and Pharmaceutical Research and Development, Merck Research Laboratories, Rahway, New Jersey 07065

Received January 16, 2009

A novel series of 1-sulfonyl-4-acylpiperazines as selective cannabinoid-1 receptor (CB1R) inverse agonists was discovered through high throughput screening (HTS) and medicinal chemistry lead optimization. Potency and in vivo properties were systematically optimized to afford orally bioavailable, highly efficacious, and selective CB1R inverse agonists that caused food intake suppression and body weight reduction in diet-induced obese rats and dogs. It was found that the receptor binding assay predicted in vivo efficacy better than functional antagonist/inverse agonist activities. This observation expedited the structure–activity relationship (SAR) analysis and may have implications beyond the series of compounds presented herein.

At least 4 of the top 10 causes of death in the U.S. and Europe are medical conditions associated with obesity, including heart disease, cancer, stroke, and type II diabetes.¹ As the rate of the overweight and obese population increases alarmingly worldwide, so does the need to reduce the incidence of obesity, a root cause of some of the more common morbidities. While healthy food choices, exercise, and a balanced life style are, in many cases, sufficient to prevent unhealthy weight gain, the same paradigm does not apply to weight loss of already overweight individuals. This paradox is mainly due to human body homeostatic energy control, a complex system of signaling and metabolic pathways responsible for promoting food intake as a means of preventing starvation.² To this end, a disruption of the homeostatic energy control, in addition to a healthy life style, is critical in reducing and maintaining reduced body weight. One point of such intervention is regulation of cannabinoid-1 receptor (CB1R^a) function, which has been the subject of intense study for several decades. While there is abundant preclinical evidence linking CB1R inverse agonism/antagonism to food intake suppression and body weight loss, this association is most convincingly supported by the results of human clinical trials of two CB1R inverse agonists, rimonabant^{3,4} and taranabant.⁵ Herein, we describe the discovery and development of a structurally diverse series of 1-sulfonyl-4-acylpiperazines as CB1R inverse agonists.

Compound **1** (Table 1) was identified through an HTS of compounds from the Merck sample collection. Interestingly, **1** exhibited potent inverse agonist activity in a CB1R functional

assay that measures cyclic-AMP (cAMP) levels^{6,7} (EC₅₀ = 1 nM) but only modest activity in a CB1R competition binding assay^{6,8} (IC₅₀ = 260nM). It had no in vivo efficacy in an overnight diet-induced obese (DIO) rat assay.^{6,9} The disparity between the binding and functional activities offered the opportunity to explore which of the two in vitro assays might be more predictive of the pharmacodynamic (PD) in vivo outcome. While the absence of in vivo efficacy of **1** did not allow for any firm conclusions because of its poor pharmacokinetics (PK) in the rat,^{6,10} it was reasonable to assume that a derivative of **1** with good PK might elucidate the disconnect between the two in vitro assays. An SAR analysis of close analogues of **1** validated the lead by establishing that its high functional activity was not due to the 3,5-bis(trifluoromethyl)benzenesulfonyl subunit, which has produced false positives from an HTS in other programs (Table 1, **2–6**). These results also confirmed that compounds **1–6** displayed the curious separation between their functional and binding in vitro activities. Compounds **1–6** did not exhibit the desired PK properties suitable for definitive evaluation in PD assays and thus for further assessment.

The chemical synthesis of derivatives of **1** was accomplished by reaction of 1-Boc-piperazine with the first coupling partner (either sulfonyl chloride R¹SO₂Cl or carboxylic acid R²CO₂H activated by EDC), followed by deprotection of the Boc group with hydrogen chloride and subsequent reaction with the second coupling partner (either sulfonyl chloride R¹SO₂Cl or carboxylic acid R²CO₂H activated by EDC) as outlined in the scheme in Table 1.

Initial optimization of **1** was primarily based on the two in vitro CB1R assays. Particular emphasis was placed on the binding assay, since many compounds were active in the functional assay and provided no real distinction for the SAR. It is noteworthy that all compounds in this series exhibited selectivity against CB2R with CB2R/CB1R in vitro activity ratios always exceeding 100 but more typically more than 1000 (e.g., hCB2 IC₅₀ values exceeded 10 μM for all key compounds depicted in Table 1, **1–5**, **33–36**). The SAR of the CB1R in vitro assays was found to be additive with respect to the structural subunits of the series, namely, the sulfonyl group,

* To whom correspondence should be addressed. Phone: +1-732-594-6624. Fax: +1-732-594-2210. E-mail: petr_vachal@merck.com.

[†] Department of Medicinal Chemistry.

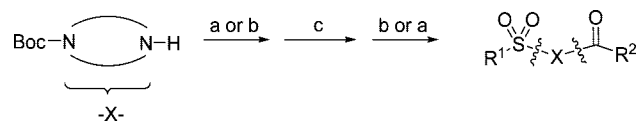
[‡] Department of Metabolic Diseases.

[§] Department of Pharmacology.

^{||} Department of Drug Metabolism/Pharmacokinetics.

[⊥] Department of Pharmaceutical Research and Development.

^a Abbreviations: CB1R, cannabinoid-1 receptor; HTS, high-throughput screening; SAR, structure–activity relationship; DIO, dietary-induced obese; EDC, 1-ethyl-3-(3-dimethylaminopropyl)carbodiimide hydrochloride; DIPEA, *N,N*-diisopropylethylamine; MED, minimal effective dose; BP, brain penetration; BW, body weight; FI, food intake; cAMP, cyclic adenosine monophosphate; PK, pharmacokinetic; PD, pharmacodynamic; RP-HPLC, reverse phase high-pressure liquid chromatography.

Table 1. CB1R Binding and Functional Activities of 1-Sulfonyl-4-acylpiperazines

Compound	R ¹ -	-X-	-R ²	CB1R IC ₅₀ ^a (nM)	CB1R EC ₅₀ ^a (nM)	Compound	R ¹ -	-X-	-R ²	CB1R IC ₅₀ ^a (nM)	CB1R EC ₅₀ ^a (nM)
1				260	1.0	19				800	2.0
2				400	1.1	20				220	0.3
3				420	0.5	21				230	2.8
4				95	0.6	22				3000	40
5				200	6.0	23				170	0.5
6				780	5.0	24				16	0.5
7				>10,000	>10,000	25				150	4.6
8				>10,000	>10,000	26				470	2.2
9				>10,000	>10,000	27				3500	>10000
10				310	7.0	28				6400	90
11				4700	180	29				9700	1500
12				290	2.5	30				9700	1500
13				700	0.6	31				9700	1500
14				2800	8.0	32				4200	>10000
15				9000	600	33				5.0	1.0
16				3100	300	34				6.0	1.0
17				>10000	900	35				5.0	1.0
18				>10000	>10000	36				1.2	1.0

^a All compounds were inverse agonists as described in ref 6.

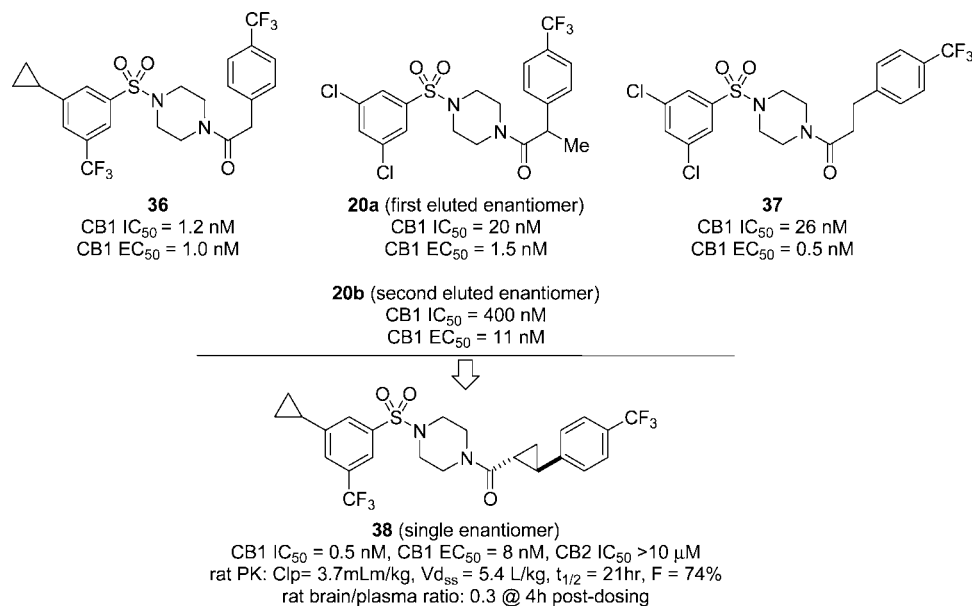


Figure 1. Design strategy of conformationally constrained CB1R inverse agonist **38**.

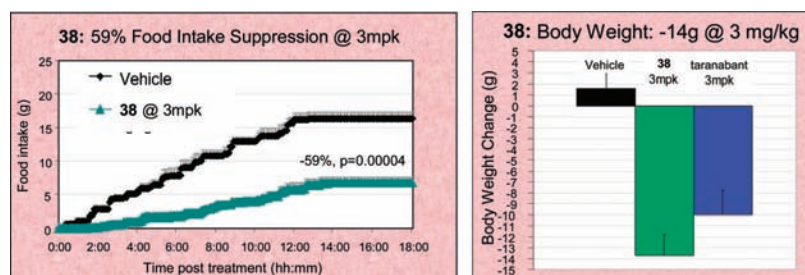


Figure 2. Effect of **38** on the overnight food intake and body weight change in DIO rats. A statistically significant food intake reduction of 59% vs vehicle was observed along with statistically significant body weight change vs vehicle, consistent with a similar effect caused by taranabant.

Table 2. Correlation of CB1R in Vitro Binding and Functional Assay to the PD DIO Rat in Vivo Efficacy Assay: PD Efficacy Consistent with Binding CB1R in Vitro Assay

	39		36		38	
	human	rat	human	rat	human	rat
Binding						
CP-55940, ^a IC ₅₀ (nM)	58	175	1.2	27	0.30	2.2
SR-141716, ^b IC ₅₀ (nM)	47	227	0.5	11	0.10	0.20
Functional Activity						
agonist EC ₅₀ (nM) (% max)	1.3 (-98%)	4.4 (-115%)	1.1 (-151%)	0.6 (-145%)	5.8 (-106%)	3.4 (-125%)
antagonist MeA ^c (% inhibition at 2 μM)	172		334		156	
MeA ^c (300 nM), IC ₅₀ (nM)		77		1.9		9.2
PD @ 3mpk (DIO rat)						
food intake change vs vehicle (%)		-14 (NS ^d)		-40		-59
absolute body weight change (g)		+8 (NS ^d)		-2		-14

^a Competition CB1R binding against CP-55940. ^b Competition CB1R binding against SR-141716. ^c Methanandamide. ^d NS = not statistically significant.

the center piperidine, and the acyl group. As such, modifications of the individual subunits did not alter the privileged structural features identified for the remaining parts of the molecule,

rendering in vitro assays very predictable when key structural features were interchanged. Structural features critical for CB1R activity included the following:

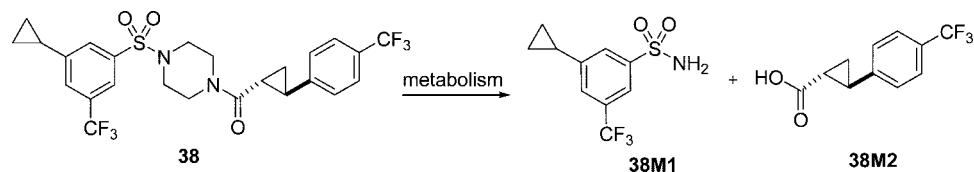
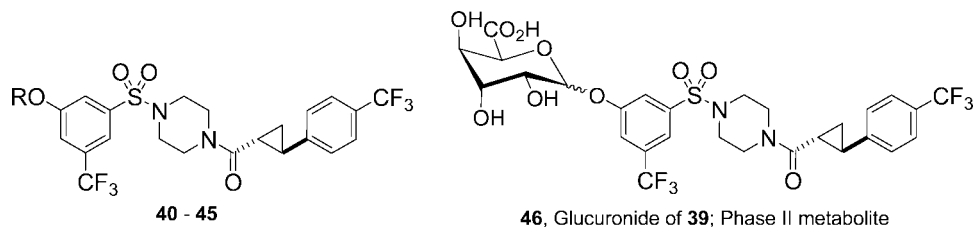


Figure 3. Metabolism of **38**. Two major metabolites were observed, **38M1** and **38M2**.

Table 3. Derivatives of **40**: Phase II Metabolism Studies in Human Hepatocytes (in Vitro)



compd	RO-	CB1R IC ₅₀ (nM)	phases II metabolite 46 observed? ^a
40	HO-	6	yes, exclusively
41	MeO-	0.5	trace
42	<i>i</i> -PrO-	0.3	no
43	<i>t</i> -Bu-OCO-	8	yes
44	EtOCO-	8	yes
45	Me ₂ NOCO-	2	yes

^a In vitro incubation in hepatocytes conducted across four species (rat, dog, monkey, and human), observation of phase II metabolite in human hepatocytes indicated therein.

(1) Sulfonamide. It was not possible to substitute the sulfonamide for conformationally less rigid functional groups or replace it with rigid isosteres, such as carboxamide.

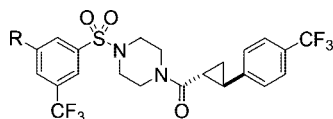
(2) Piperazine Ring. Replacement of the central piperazine with piperidine, pyrrolidine, or either regioisomer of 3-aminoazetidine produced inactive compounds (Table 1, **7–9** vs **33**). It was found that the piperazine ring underwent metabolic oxidation as assessed in liver microsome incubations. In an attempt to improve the metabolic stability of the piperazine ring, 2- and 3-substituted analogues were prepared. While monosubstitution and disubstitution of the 3-position with relatively small groups (**10**, **12**) were tolerated, 2-substitution and 3,5-disubstitution generally reduced CB1R activity (**13–17**). More importantly, there was no improvement in PK properties by piperazine substitutions.

(3) Carboxamide. Replacement with methylene (i.e., *N*-cyclohexylmethyl) derivative) or complete omission of the carboxamide functionality (i.e., *N*-alkyl- and *N*-arylpiperidine derivatives) failed to display any CB1R activity in vitro. It is also noteworthy that the carboxamide was not interchangeable with sulfonamide, implying that its role extended beyond just structural rigidity (analogue of **1** in which the carboxamide was replaced with sulfonamide was inactive up to 10 μM in both in vitro assays). Along with the need for presence of the sulfonamide on the second piperazine nitrogen, these data suggested that the molecules bound to the CB1R in a specific orientation and the two sides of the molecule were not interchangeable. Carboxamides derived from aromatic carboxylic acids were found to exhibit inferior binding compared to their aliphatic counterparts (e.g., Table 1, compare **1** vs **18**). On the other hand, CB1R active aliphatic carboxamides represented a metabolic liability as they underwent rapid oxidation of their aliphatic side chains. This liability was overcome by introducing metabolically more robust aromatic substituents separated from the carbonyl functionality with a methylene spacer. The resulting hybrid derivative (e.g., **19**) proved much more stable (both in vitro in liver microsomes and in vivo PK) while maintaining strong CB1R functional properties in vitro. Metabolic stability of the

benzylic α-carboxamide methylene could be further enhanced by substitution (**20**, **21**) or by deactivation with electron-withdrawing functionalities (**22–24**). The latter also proved beneficial for CB1R binding and functional activity (compare **24** vs **19**). Electron-withdrawing groups in the 4-position were found to be superior relative to 2- and 3-substitutions (**24** vs **25** and **26**).

(4) Arylsulfonamide. While good in vitro activity was limited to arylsulfonamides, some degree of flexibility was observed with a range of aryl substituents (Table 1, **1–6**). Initially, 3,5-disubstitution of the aryl ring proved to be superior to other mono-, bis-, and trisubstitution patterns (e.g., **6** vs **27–31**; **1** vs **32**). Generally, electron-deficient arylsulfonamides were slightly more active in vitro and also enhanced piperazine ring oxidative stability, thus providing improved overall PK profiles as evidenced by **33** (rat PK: Cl_p = 37 (mL/min)/kg, V_{dss} = 9.6 L/kg, t_{1/2} = 6.1 h, F = 20%). To this end, a single 3-trifluoromethyl substituent of arylsulfonyl ring caused the aromatic ring to be sufficiently stable to rapid oxidation. Of several 5-positional derivatives of **33**, exemplified by **34** and **35**, the best combination of potent in vitro activity with modest in vivo stability was observed for the 5-cyclopropyl-3-trifluoromethyl derivative **36** (Tables 1 and 2).

The additive nature of the SAR for individual subunits of the lead structure was further exploited to advance the series. Initially, while compound **36** was the best example of balanced functional and binding CB1R in vitro activities, its overall properties were still suboptimal, as it afforded only a modest food intake reduction in the DIO rat assay. Second, the role of α-methylene substitution was evaluated by resolving the racemic α-methyl compound **20** (Table 1). The two resulting enantiomers, **20a** and **20b**, displayed vastly different activities in vitro (Figure 1). Finally, compound **37** exhibited in vitro profile similar to **20a**, suggesting that a two carbon spacer might be superior to the one carbon spacer. The inherent potential of the ethylene linker might also have been somewhat compromised by its flexibility. The combination of these three features (namely, the 3,5-disubstitution pattern in **36**, the configuration

Table 4. Derivatives with the Potential for Formation of Phase II Conjugates in Hepatocytes

Compound	R-	CB1R IC ₅₀ ^a (nM)	In vitro Ph II Metabolite?	Body weight change (g) ^b	hERG IC ₅₀ ^d (μM)
47		4	No	No effect ^c	0.9
48		8	No	No effect ^c	1.2
49		5	No	N/A	2.5
50		1.5	Trace amount	-8g	0.06
51		0.7	No	N/A	N/A
52		0.6	No	N/A	N/A
53		7	No	N/A	N/A
54		50	N/A	N/A	N/A
55		0.3	No	N/A	1.2
56		0.3	Trace amount	-10g	0.5
57		9	No	No effect ^b	0.5
58		20	No	No effect ^b	0.04
59		200	Yes	N/A	N/A
60		100	Yes	N/A	N/A
61		400	Yes	N/A	N/A
62		400	Yes	N/A	N/A
63		10	Yes	No effect ^c	4.0
64		3	Yes	No effect ^c	3.5
65		0.2	Yes	-14g	1.1
66		10	No	No effect ^c	1.3

^a hCB2 IC₅₀ exceeded 10 μM for all compounds reported in Table 4.

^b Acute overnight body weight change in DIO rat at 3 mpk. ^c Not statistically significant vs vehicle. ^d MK0499 binding assay.

preference in **20a**, and the two carbon spacing of **37**) led to the design of conformationally constrained **38** which provided optimal in vitro binding and functional properties and significantly improved PK and brain penetration in the rat. Compound **38** caused a robust overnight food intake reduction in DIO rats resulting in a very significant body weight decrease compared

to vehicle treated animals. This result finally validated the potential of this series of compounds (Figure 2). The ability of **38** to reduce body weight was further demonstrated in a DIO dog model (2% overall body weight reduction at 2 (mg/kg)/day po after 5 days; data not shown).⁶

While the magnitude of the functional and binding CB1R in vitro assays converged for some of the most active compounds of the series (Table 1, **34–36**), the disparity of the two assays observed for the majority of examples listed in Table 1 remained of interest. An effort was devoted to connect one of the two often divergent assays to the primary PD assay and thus to in vivo efficacy. Table 2 outlines a series of three closely related analogues (**36**, **38**, and **39**) of which most in vitro and in vivo characteristics were found to be remarkably similar. All three compounds had similar functional activity in vitro (EC₅₀) and were similarly potent inverse agonists. They had similar rat PK properties and similar brain penetration (brain/plasma ratio, or b/p), an important attribute given the strong CB1R expression in the brain. The three compounds differ only in the values of the in vitro binding potency (IC₅₀) in competition assays employing different ligands ([³H]CP-55,940 or [³H]SR141716). The significant differences among the compounds enabled a convincing comparison of otherwise remarkably similar compounds, differing only in their binding. The effect on body weight decrease and food intake suppression in the DIO rat model increased with increased binding potency: **38** > **36** > **39**, respectively. The correlation was consistent with the binding assay being more reliably predictive of in vivo efficacy. This conclusion not only rationalized the lack of efficacy of the many strongly functionally active compounds outlined in Table 1 but it also expedited subsequent SAR analysis, enabling us to focus on binding rather than functional activity as the more reliable predictor of compounds which may be more suitable for further in vivo evaluation.

Isolation of metabolites in rats and dogs established oxidation of the piperazine ring as the primary metabolism of **38** (Figure 3). Two major metabolites, **38M1** and **38M2**, were observed, neither of which had any significant activity against CB1R in vitro. While plasma half-life of the acid **38M2** was short-lived and cleared rapidly, the primary sulfonamide **38M1** accumulated in circulation in both rats and dogs. Comparison of human metabolism to rat and dog in vitro suggested that a similar profile, including long-lived **38M1**, was likely to be observed in humans. The potential of encountering serious issues associated with a long-lived metabolite such as **38M1** in late stage development prompted a focused effort to alter the PK profile of the lead by substituting the arylsulfonamide with a metabolically labile functional group which might prevent metabolite accumulation by increasing its rate of clearance. It was clear from the SAR that such a functionality should be introduced in the 5-position of arylsulfonamide, replacing the cyclopropyl residue, in order to maintain both CB1R activity and overall in vivo PK stability. Both 3,5-substitution with at least one being a CF₃ group had been established (see discussion of Table 1). Initially, derivatives bearing functionality capable of undergoing phase II metabolism in vitro (i.e., forming a glucuronide adduct) were surveyed.

Phenol **40** underwent rapid glucuronidation when incubated in hepatocyte homogenates from several species (rat, dog, monkey, and human) to produce glucuronide **46** as the major metabolite (Table 3). While phenol **40** could not be considered as a development candidate for numerous reasons, including poor oral bioavailability in rats, derivatives of **40** that would release the parent phenol **40** in vivo as well as any primary

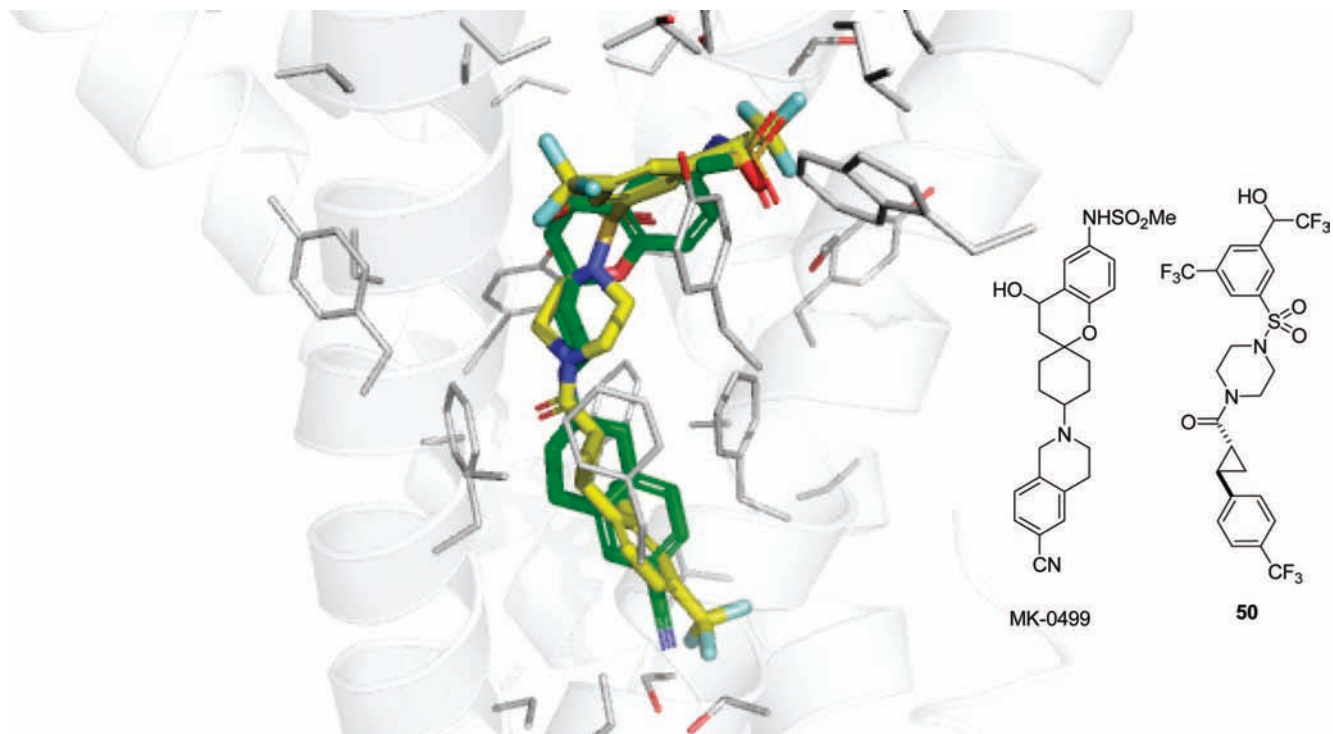
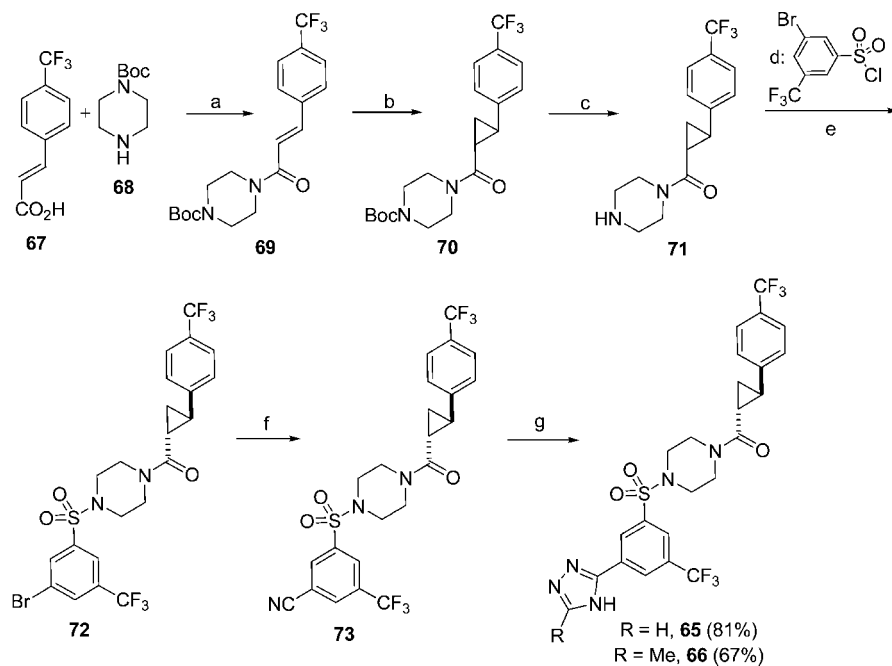


Figure 4. Overlay of compound **50** (yellow) with MK0499 (green) in a model of the potassium hERG channel indicated a significant degree of similarity of the two compounds consistent with a strong hERG activity observed for **50**.

Scheme 1. Synthesis of **65** via Distereoselective Cyclopropanation and Direct 1,3,4-Triazole Formation^a



^a Conditions: (a) EDC, DIPEA; (b) $\text{Me}_3\text{S(O)I}$, NaH, DMSO, 40°C, *E/Z* > 50:1; (c) 4 M HCl in dioxane; (d) sulfonyl chloride (see scheme for its structure), aq NaHCO_3 , DCM; (e) chiral separation, Chiralcel AD, 35% yield (five steps), single enantiomer; (f) $\text{Zn}(\text{CN})_2$, $\text{Pd}_2(\text{dba})_3$, dppf, DMF, 115°C, 74%; (g) RCOHNH_2 , DMF/NMP (1/1), 140 °C.

sulfonamide metabolite analogous to **38M1** (Figure 3) were prepared. Simple alkyl ethers (**41**, **42**), which were affording a robust body weight reduction in DIO rats, did not undergo efficient dealkylation to produce **40**. On the other hand, carbonates **43** and **44** and carbamate **45** all rapidly produced **40** and thus glucuronide **46** but were only marginally efficacious in the DIO rat model.

Alcohols **47–50** represented another class of derivatives with the potential to form phase II conjugates (Table 4). Trifluoromethyl alcohol **50** produced trace amounts of a glucuronide adduct in hepatocyte incubations and was efficacious in the acute DIO rat model at 3 mg/kg po. Counterscreening revealed a very strong affinity of **50** to potassium channel (hERG) and as such was not considered as a viable lead. It served, however, as an

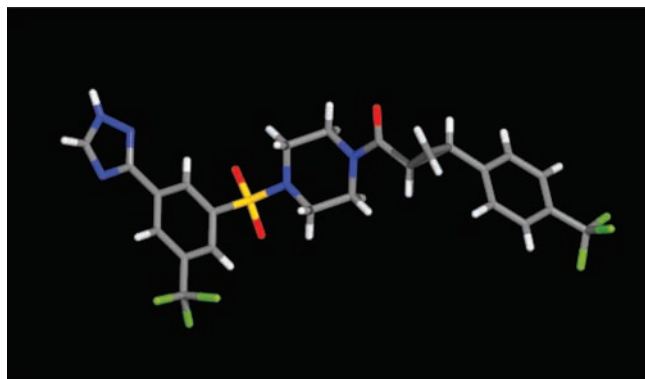
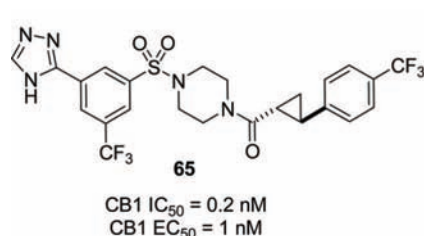


Figure 5. X-ray crystallography analysis determined the absolute stereochemistry of the cyclopropane ring of **65** as (*R,R*).

important tool in establishing key features responsible for its high affinity for hERG channel. Figure 4 depicts a computational docking model comparing **50** to MK0499, a strong ligand of hERG used as a standard in many hERG binding assays. This modeling exercise suggested qualitatively that a polar R substituent might disrupt the high affinity for hERG resulting from the apparent binding interaction of the trifluoromethyl group of **50** with lipophilic residues of hERG.

Heterocycles containing polar functionalities represent attractive targets by having the potential for exhibiting both phase II conjugation and lowering the observed hERG activity. Numerous heterocyclic derivatives were prepared and found to differ vastly in their ability to interact with CB1R (Table 4, **51–66**). Compounds active in the binding assay were tested for their ability to form phase II conjugates by incubations in human hepatocytes. Contrary to our expectations, the vast majority of heterocycles failed to produce phase II conjugates. Only four heterocyclic derivatives that displayed both in vitro binding to CB1R and the potential for glucuronidation were identified (**56**, **63–65**). Of these four, only **56** and **65** proved efficacious in the acute overnight DIO rat model, causing robust body weight change and food intake suppression at a dose of 3 mg/kg po. The 1,3,4-triazole derivative **65** had a superior profile demonstrating CB1R potency, activity in DIO rats, and reduced hERG activity ($IC_{50} > 1 \mu M$).



DIO Rat FI: MED ~ 0.3 mpk

Strong PhII conj. (Human hepatocytes)

brain/plasma = 0.2 @ 4h post-dosing

CYP3A4 = 4.7 μM

CYP2D6 = 6.0 μM

CYP2C9 = 11 μM

CYP2C8 = 15 μM

hERG = 1.0 μM

PAN labs: 0 hits < 1 μM ; 5 hits < 10 μM

Pharmacokinetics of 65			
Species	Rat	Dog	Monkey
Cl_b	23.7	1.4	14.6
Vd_{ss}	3.8	1.1	2.5
$t_{1/2}$	3.8h	8.6h	2.0h
C_{max}	0.19 μM	0.21 μM	0.003 μM
F	31%	26%	<2%

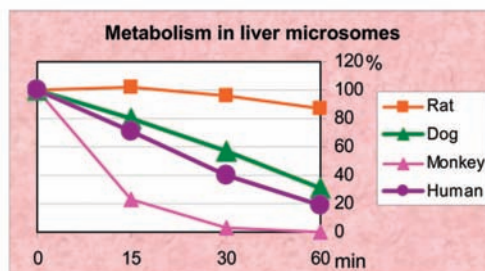


Figure 6. In vitro and in vivo characterization of **65**. Primary PD assay established MED as 0.3 mpk. Off-target activity was assessed by PAN laboratory screen, CYP panel inhibition assays, and hERG (vs MK499). In vivo characterization included PK across three preclinical species and brain PK in the rat.

Novel chemistry was developed for the synthesis of **65**. A reaction of nitriles with hydrazides should theoretically produce the desired 1,3,4-triazoles upon heating. However, we found no example of such reactivity described in the literature. Intrigued by the potential simplicity of this single-step process, we screened several solvents and found that heating formylhydrazide with nitrile **73** in a DMF/NMP mixture produced the desired **65** in 81% isolated yield (Scheme 1). This novel reactivity extended to other substrates as exemplified by reaction of **73** with acethydrazide to afford **66**. While the reaction is likely limited to strongly electron-deficient nitriles, it does provide an attractive solution for derivatives of **65** serving as the primary synthetic route to multigram quantities of the compound (Scheme 1). Another noteworthy chemical reactivity arose from the application of the Corey–Chaykovsky cyclopropanation¹¹ to amides. Cyclopropanation of esters, for which the Corey–Chaykovsky cyclopropanation was developed and mostly utilized, proceeds generally with relatively low levels of diastereomeric control. When applied to cyclopropanation of methyl cinnamates in the context of our series, an *E/Z*-cyclopropane ratio of 2/1 was obtained. However, when cyclopropanation was applied to amide **69**, the reaction proceeded with excellent selectivity forming the desired *E*-isomer exclusively (*E/Z* > 50/1). This discovery significantly expedited preparation of a larger quantity of **65** necessary for full in vivo and in vitro characterization (Scheme 1). Finally, absolute stereochemistry of **65** was determined as (*R,R*) by means of single X-ray crystallography analysis (Figure 5).

Triazole **65** was evaluated in a series of in vivo and in vitro experiments (Figure 6). The minimal effective dose (MED) causing statistically significant body weight reduction and food intake suppression in DIO rat was determined to be 0.3 mpk. 1,3,4-Triazole **65** exhibited a very clean profile in a broad counterscreen, displaying no off-target activities ($IC_{50} \geq 1 \mu M$). The strong signal of the primary glucuronide of **65** formed in hepatocyte homogenates across four species was anticipated to provide a sufficient clearance mechanism for **65** and its potential sulfonamide metabolites. Pharmacokinetic studies of **65** established good profile in rats and dogs but revealed an unexpectedly low oral bioavailability in rhesus monkey (Figure 6). Metabolic stability of **65** in liver microsomal incubations revealed that the

stability of **65** in human microsomes fell between that of dogs and rhesus monkeys. As such, these results raised some ambiguity about the stability of **65** in human. The potential risk of poor PK in humans ultimately rendered the final decision to discontinue further investigation of the piperazine series as a treatment of obesity in human.

In conclusion, a novel series of highly efficacious and target specific CB1R inverse agonists, exemplified by **65**, was developed. Numerous compounds in this series caused significant body weight reduction and food intake suppression in two preclinical species, DIO rats and dogs. During the development process, an important causality link between the primary binding and in vivo efficacy was established, not only effectively advancing the series described herein but providing a basis for expedited SAR optimization for other CB1R inverse agonist leads. Careful profiling of in vitro and in vivo characteristics, including receptor potency, off-target activity, and designed metabolic pathways for clearance, led to the identification of a unique series of potent inhibitors of the CB1R with many desirable properties.

Experimental Section

General. Unless specified otherwise, all materials were purchased from commercial sources and used as received. ^1H and ^{13}C NMR spectra were recorded using a Bruker 400 MHz instruments. Preparative reverse phase liquid chromatography (RP HPLC) was performed using Waters MS directed purification system consisting of 2525 binary gradient pump, 2767 injector/collector, and 2996 PDA UV detector, mobile phase consisting of a gradient of water and acetonitrile (each cont. 0.1% TFA), and a Waters Xterra column (50 mm \times 3 mm, 3.5 μm packing material). The purity of **1–72** has been determined by HPLC analysis (electrospray positive ionization, Micromass ZQ single quadrupole)¹² as $\geq 95\%$ for **1–69** and **72** and as 90% for **70** and **71** (see the detailed experimental procedure for the discussion of the purity of **70** and **71**). Preparation of compound **4** represents a typical procedure used for the synthesis of compounds disclosed therein:

Sulfonamide Formation. To a solution of 1-naphthylsulfonyl chloride (300 mg, 1.32 mmol) in anhydrous acetonitrile (25 mL), triethylamine (2.6 mmol) and *tert*-butylpiperazine-1-carboxylate (2.6 mmol) were added sequentially with stirring. The reaction mixture was stirred at room temperature for 2 h, concentrated, and the crude oily residue was dissolved in ethyl acetate (100 mL). The solution was washed sequentially with an aqueous solution of hydrochloric acid (0.25 M, 100 mL) and aqueous solution of sodium hydroxide (1 M, 50 mL), dried with sodium sulfate, and concentrated to afford *tert*-butyl 4-(1-naphthylsulfonyl)piperazine-1-carboxylate as a white solid (456 mg, 1.21 mmol, 91% yield): LCMS m/z (MH - Boc)⁺ = 277 at 2.21 min; ^1H NMR (CDCl₃, 500 MHz) δ 8.8 (d, J = 8.7 Hz, 1H), 8.2 (d, J = 7.5 Hz, 1H), 8.1 (d, J = 8.0 Hz, 1H), 7.9 (d, J = 8.0 Hz, 1H), 7.6 (t, J = 7.1 Hz, 1H), 7.6 (m, 2H), 3.5 (m, 4H), 3.2 (m, 4H), 1.4 (s, 9H).

Boc Deprotection. *tert*-Butyl 4-(1-naphthylsulfonyl)piperazine-1-carboxylate (400 mg, 1.22 mmol) was dissolved in a 20% (v/v) solution of trifluoroacetic acid in dichloromethane (10 mL) and the resulting solution stirred at room temperature for 2 h and concentrated. The resulting crude residue was dissolved in dichloromethane, washed with 1 M solution of sodium hydroxide, dried with sodium sulfate, and concentrated to afford 1-(1-naphthylsulfonyl)piperazine as a white solid (256 mg, 1.12 mmol, 92%): LCMS m/z (MH)⁺ = 277; ^1H NMR (CDCl₃, 500 MHz) δ 8.8 (d, J = 8.4 Hz, 1H), 8.2 (d, J = 7.3 Hz, 1H), 8.1 (d, J = 8.2 Hz, 1H), 7.9 (d, J = 7.8 Hz, 1H), 7.6 (t, J = 6.9 Hz, 1H), 7.5 (m, 2H), 3.2 (m, 4H), 2.9 (m, 4H).

Carboxamide Formation (4). To a solution of 1-(1-naphthylsulfonyl)piperazine (250 mg, 1.1 mmol) in anhydrous dichloromethane (10 mL), cyclopropylcarboxylic acid (2.0 mmol) and *N*-(3-dimethylaminopropyl)-*N'*-ethylcarbodiimide hydrochloride (edc chloride, 2.0 mmol) and diisopropylethylamine (5.0 mmol) were

added sequentially with stirring. The reaction mixture was stirred at room temperature for 2 h, concentrated, and purified using RPHPLC to afford 1-(cyclohexylcarbonyl)-4-(1-naphthylsulfonyl)piperazine **4** as colorless oil (0.73 mmol, 66% yield): LCMS (method A) m/z (MH)⁺ = 387.1 at 2.19 min; ^1H NMR (CDCl₃, 500 MHz) δ 8.8 (d, J = 8.5 Hz, 1H), 8.2 (d, J = 7.5 Hz, 1H), 8.1 (d, J = 8.3 Hz, 1H), 7.9 (d, J = 8.0 Hz, 1H), 7.7 (t, J = 8.4 Hz, 1H), 7.6 (m, 2H), 4.7 (m, 1H), 3.6 (m, 4H), 3.5 (m, 4H), 3.2 (m, 4H), 1.4 (m, 4H), 1.2 (m, 6H).

Detailed Experimental Procedure of the Key Compound 65. **69.** *N,N*-Diisopropylmethylamine (0.3 mol) was added to a mixture of (2*E*)-3-[4-(trifluoromethyl)phenyl]acrylic acid (**67**, 21.6 g, 0.10 mol), 1-(1-naphthylsulfonyl)piperazine (**68**, 0.10 mmol), *N*-(3-dimethylaminopropyl)-*N'*-ethylcarbodiimide hydrochloride (edc hydrochloride, 2.0 mmol) in anhydrous dichloromethane (300 mL) via syringe at room temperature over 10 min and allowed to stir at ambient temperature for additional 30 min. The mixture was transferred into a separatory funnel, diluted with additional dichloromethane (300 mL), and washed sequentially with 1 M aqueous hydrochloric acid (500 mL), 1 M aqueous sodium hydroxide (500 mL), and brine (500 mL), dried over sodium sulfate, filtered, and concentrated yielding **69** as 37 g of a white solid used in the subsequent step without further purification (0.097 mol, 97%, >97% pure by LCMS): LCMS (method A) m/z (MH)⁺ = 285.1, 329.2 at 3.42 min.

70. Sodium hydride (60% w/w in mineral oil, 0.15 mol) was added to a solution of trimethylsulfoxonium iodide (0.15 mol) in DMSO (600 mL) at 40 °C over 5 min under an inert atmosphere of nitrogen in oven-dried glassware. The reaction mixture was stirred at ambient temperature for 30 min at 40 °C, and **69** (37 g, 0.097 mol) was added in a single portion. The resulting mixture was heated to 40 °C for additional 15 h, poured onto ice (1 L), and extracted with ether (1 L). The aqueous layer was extracted with ethyl acetate (2 \times 200 mL). Combined organic layers were washed sequentially with 1 M aqueous hydrochloric acid (500 mL), 1 M aqueous sodium hydroxide (500 mL), and brine (500 mL), dried over sodium sulfate, filtered, and concentrated, yielding **70** as 36.8 g of a white solid used in the subsequent step without further purification (90% pure¹³ by LCMS): LCMS (method A) m/z (MH)⁺ = 299.2 at 3.54 min.

71. A 4 M solution of hydrogen chloride in dioxane (400 mL) was added to **70** (36.8 g 90% purity) and the resulting mixture was stirred at ambient temperature for 0.5 h, concentrated, and flushed with toluene (0.5 L), yielding **71** as a clear oil: LCMS (method A) m/z (MH)⁺ = 299.2 at 2.23 min.

3-Bromo-5-(trifluoromethyl)benzenesulfonyl chloride (0.11 mmol) was added to a vigorously stirred mixture of **71**, dichloromethane (500 mL), and saturated aqueous solution of sodium bicarbonate (500 mL). The resulting mixture was stirred at ambient temperature for 1 h, the organic layer was separated, and the aqueous layer was extracted with dichloromethane (200 mL). Combined organic layers were dried over sodium sulfate, filtered, and concentrated. The crude product was purified by a filtration through a silica gel column (eluent: gradient of ethyl acetate in heptane 0–50%) and concentrated, yielding 42 g of white solid. Chiral separation was performed using Chiracel AD column (eluent: 12% solution of 2-propanol in heptane); the desired (*R,R*)-enantiomer **71** was collected as the second eluted isomer (20.2 g, 0.035 mol, >95% purity by LCMS, 35% overall yield from **67**). LCMS (method A) m/z (MH)⁺ = 585, 587 at 3.98 min; ^1H NMR (CDCl₃, 500 MHz) δ 1.37 (m, 1H), 1.66 (m, 1H), 1.90 (m, 1H), 2.49 (m, 1H), 3.22 (m, 4H), 3.60 (m, 4H), 7.20 (d, J = 16 Hz, 2H), 7.50 (d, J = 16 Hz, 2H), 8.50 (s, 1H), 8.68 (s, 1H), 8.80 (s, 1H).

72. A mixture of **71** (2.93 g, 5 mmol), zinc(II) cyanide (5 mmol), 1,1'-bis(diphenylphosphine)ferrocene (0.27 mmol), tris(dibenzylideneacetone)dipalladium (0.11 mmol), *N,N*-dimethylformamide (99 mL), and water (1 mL) was combined, and the resulting mixture was degassed with a stream of nitrogen bubbled through the solution at ambient temperature with stirring for 1 h and then heated to 115 °C for 30 min. The resulting solution was combined with ether (200 mL) and washed with deionized water (2 \times 100 mL), dried

with sodium sulfate, concentrated, and purified using column chromatography on silica gel (Biotage 40S, 10–100% ethyl acetate in hexane) to afford **72** as a white solid (3.7 mmol, 74%): LCMS (method A) m/z (MH)⁺ = 532.1 at 3.58 min; ¹H NMR (CDCl₃, 500 MHz) δ 1.34 (m, 1H), 1.60 (m, 1H), 1.97 (m, 1H), 2.57 (m, 1H), 3.20 (m, 4H), 3.80 (m, 4H), 7.15 (d, J = 16 Hz, 2H), 7.53 (d, J = 16 Hz, 2H), 8.55 (s, 1H), 8.71 (s, 1H), 8.80 (s, 1H).

65. A mixture of **73** (1.60 g, 3 mmol), formylhydrazide (12 mmol), *N,N*-dimethylformamide (10 mL), and *N*-methylpyrrolidine (10 mL) was heated to 140 °C for 15 h, transferred to a silica gel column, and purified by a column chromatography (Biotage 40S, 10–100% ethyl acetate in hexane) to afford **65** as a white solid (1.40 g, 2.43 mmol, 81%): LCMS (method A) m/z (MH)⁺ = 574.2 at 3.42 min; ¹H NMR (CDCl₃, 500 MHz) δ 1.34 (m, 1H), 1.66 (m, 1H), 1.92 (m, 1H), 2.53 (m, 1H), 3.20 (m, 4H), 3.79 (m, 4H), 7.15 (d, J = 16 Hz, 2H), 7.53 (d, J = 16 Hz, 2H), 8.07 (s, 1H), 8.54 (s, 1H), 8.63 (s, 1H), 8.75 (s, 1H). X-ray analysis of **65** (Figure 5): C₂₄H₂₁F₆N₅O₃S, M_r = 573.530, monoclinic, $P2_1$, a = 4.8910(7) Å, b = 21.155(3) Å, c = 14.292(2) Å, β = 99.123(2)°, V = 1460.1(4) Å³, Z = 2, D_x = 1.304 g cm⁻³, monochromatized radiation λ (Mo) = 0.710 73 Å, μ = 0.18 mm⁻¹, $F(000)$ = 588, T = 100 K. Data were collected on a Bruker CCD diffractometer to a θ limit of 27.81° which yielded 19 071 reflections. There are 6900 unique reflections with 5126 observed at the 2 σ level. The structure was solved by direct methods (SHELXS-97; Sheldrick, G. M. *Acta Crystallogr.*, **1990**, *A46*, 467–473) and refined using full-matrix least-squares on F^2 (Sheldrick, G. M. SHELXL-97. Program for the Refinement of Crystal Structures, University of Göttingen, Germany). The final model was refined using 363 parameters and all 6900 data. All non-hydrogen atoms were refined with anisotropic thermal displacements. The final agreement statistics are as follows: R = 0.087 (based on 5126 reflections with $I > 2\sigma(I)$), wR = 0.224, S = 1.15 with $(\Delta/\sigma)_{\max}$ = 0.03. The maximum peak height in a final difference Fourier map is 1.402 e Å⁻³ and possibly associated with disordered and unresolved solvent. CCDC contains the supplementary crystallographic data for this paper (CCDC deposition number 721736). These data can be obtained free of charge from The Cambridge Crystallographic Data Centre via www.ccdc.cam.ac.uk/data_request/cif.

Supporting Information Available: Description of biological assays, characterization of compounds **1–72**, synthetic procedures, and X-ray crystallographic analysis data of **65**. This material is available free of charge via the Internet at <http://pubs.acs.org>.

References

- Center of Disease Control Web site: <http://www.cdc.gov/nchs/FASTATS/lcod.htm>.
- Morton, G. L.; Cummings, D. E.; Baskin, D. G.; Barsh, G. S.; Schwartz, M. W. Central nervous system control of food intake and body weight. *Nature (London)* **2006**, *443*, 289–295.
- (a) Di Marzo, V.; Goparaju, S. K.; Wang, L.; Liu, J.; Bitkai, S.; Jarai, Z.; Fezza, F.; Miura, G. I.; Palmiter, R. D.; Sugiura, T.; Kunos, G. Leptin-regulated endocannabinoids are involved in maintaining food intake. *Nature (London)* **2001**, *410*, 822–825. (b) Van Gaal, L. F.; Rissanen, A. M.; Scheen, A. J.; Ziegler, O.; Roessner, S. Effects of the cannabinoid-1 receptor blocker rimonabant on weight reduction and cardiovascular risk factors in overweight patients: 1-year experience from the RIO-Europe study. *Lancet* **2005**, *365*, 1389–1397.
- Rimonabant was approved for the treatment of obesity in the European Union in 2006. For more information, see <http://en.sanofi-aventis.com/events/event1/en/about.asp>.
- Addy, C.; Li, S.; Agrawal, N.; Stone, J.; Majumdar, A.; Zhong, L.; Li, H.; Yuan, J.; Maes, A.; Rothenberg, P.; Cote, J.; Rosko, K.; Cummings, C.; Warrington, S.; Boyce, M.; Gottesdiener, K.; Stoch, A.; Wagner, J. Safety, tolerability, pharmacokinetics, and pharmacodynamic properties of taranabant, a novel selective cannabinoid-1 receptor inverse agonist, for the treatment of obesity: results from a double-blind, placebo-controlled, single oral dose study in healthy volunteers. *J. Clin. Pharmacol.* **2008**, *48*, 418–427.
- For a detailed discussion of biological assays, see the following: Fong, T. M.; Guan, X.-M.; Marsh, D. J.; Shen, C.-P.; Stribling, D. S.; Rosko, K. M.; Lao, J.; Yu, H.; Feng, Y.; Xiao, J. C.; Van der Ploeg, L. H. T.; Goulet, M. T.; Hagmann, W. K.; Lin, L. S.; Lanza, T. J.; Jewell, J. P.; Liu, P.; Shah, S. K.; Qi, H.; Tong, X.; Wang, J.; Xu, S. S.; Francis, B.; Strack, A. M.; MacIntyre, D. E.; Shearman, L. P. Antiobesity efficacy of a novel cannabinoid-1 receptor inverse agonist, *N*-[1-(1S,2S)-3-(4-chlorophenyl)-2-(3-cyanophenyl)-1-methylpropyl]-2-methyl-2-[[5-(trifluoromethyl)pyridin-2-yl]oxy]propanamide (MK-0364), in rodents. *J. Pharmacol. Exp. Ther.* **2007**, *321*, 1013–1022.
- In vitro CB1R and CB2R functional activity of a test compound was measured by incubating recombinant CB1R-CHO cells with various concentrations of the test compound in the presence of 10 mM forskolin, 200 mM phosphodiesterase inhibitor, 3- isobutyl-1-methylxanthine (IBMX) in the assay buffer (Earle's balanced salt solution supplemented with 5 mM MgCl₂, 10 mM HEPES, pH 7.3, 1 mg/mL BSA) at room temperature for 30 min. Cells were lysed by boiling, and intracellular cAMP level was determined using the cAMP SPA kit (Amersham). When adenylyl cyclase is activated by forskolin, activation of Gi by CB1R in the presence of agonist (such as CP55940) will lead to an inhibition of the forskolin-stimulated cAMP increase, and inverse agonist will lead to a further increase of the forskolin-stimulated cAMP increase. The maximal CP55940-mediated inhibition of forskolin-stimulated cAMP increase is defined as 100% agonist efficacy, and the intrinsic activity of all other compounds is relative to the efficacy of CP55940. Negative efficacy denotes inverse agonism.
- In vitro CB1R and CB2R binding assays were performed by incubating various concentrations of a test compound with 0.5 nM [³H]CP55940, 1.5 g of recombinant human CB1R-CHO membranes (or 0.1 mg of human CB2R-CHO membranes) in 50 mM Tris-HCl, pH 7.4, 5 mM MgCl₂, 2.5 mM EDTA, 0.5 mg/mL fatty acid free bovine serum albumin (BSA), 1 × proteinase inhibitor mix (P8340, Sigma), and 1% DMSO. After 1 h of incubation at 37°C, the reaction was stopped by filtration and bound radioligand was separated from free radioligand by washing the filter plate. Total specifically bound radiolabel was 10% or less of the total added radiolabel. Inhibitory IC₅₀ values were calculated through nonlinear curve fitting.
- Food intake assays. For automated food intake system, Sprague–Dawley CD and DIO (dietary-induced obese Sprague–Dawley CD) rats (obtained from Charles River Labs; Wilmington, DE) were caged individually in Nalgene cages with metabolism feeders attached to them. The food cups were external to the feeder and were placed on individual balances. Each balance was connected to a central computer that collects readings every 5 min to measure grams of food consumed. Rats were transferred into the AFIS for at least 3 days before the experiment to allow for acclimation. For overnight food intake (FI) and body weight (BW) assay, male DIO rats were orally gavaged at 1 h prior to dark cycle onset with vehicle (10% Tween-80 in water) or the CB1R inverse agonist. Rats were fed milled MHF diet during acclimation to the caging and during the experiment. Overnight food intake and body weight changes were measured. Significance level was set at $P < 0.05$.
- Pharmacokinetic assays. Male Sprague–Dawley rats (Taconic Farms, Germantown, NY) were dosed intravenously at 1 mpk and orally at 2 mpk for pharmacokinetic (PK) evaluations. The blood samples were collected at various time points into lithium heparin tubes and centrifuged. The plasma samples were kept at –70 °C until analysis. For brain penetration (BP) study, the male Sprague–Dawley rats were administered intravenously at 1 mpk and 1 h later euthanized by CO₂ asphyxiation. The whole brain was collected, frozen on dry ice, and stored at –70 °C. Blood was collected via cardiac puncture into lithium heparin tubes and treated the same way as PK study. The plasma samples were extracted by protein precipitation and analyzed by LCMS². The whole rat brain was homogenized, and was then extracted by protein precipitation prior to LCMS² analysis.
- Corey, E. J.; Chaykovsky, M. Dimethylloxosulfonium methylyde and dimethylsulfonium methylyde. Formation and application to organic synthesis. *J. Am. Chem. Soc.* **1965**, *87*, 1353–1364.
- Mass Spectrometer: Micromass ZQ single quadrupole, electrospray positive ionization, full scan mode (150–750 amu in 0.5 s). HPLC: Agilent 1100, binary pump. DAD UV detector: hardware/software Waters/Micromass MassLynx 4.0. Column: Waters Xterra, 2.1 mm width, 20 mm length, 3.5 μ m packing material. Run time: 4 min. Flow rate: 1.0 mL/min. Mobile phase A = water + 0.05% TFA. Mobile phase B = acetonitrile + 0.05% TFA. Gradient, time/% A/% B: 0.00/95/05, 3.00/2/98, 3.25/2/98, 3.26/95/5, 4.00/95/5.
- The final crude product **70** contains approximately 10% of *tert*-butyl 4-{3-[4-(trifluoromethyl)phenyl]butanoyl}piperazine-1-carboxylate byproduct which does not negatively affect the subsequent steps; E/Z ratio of **70** is >50/1.

JM900063X